

In situ synthesis and modification of cotton fibers with bismuthoxychloride and titanium dioxide nanoparticles for photocatalytic applications

V.C. Ferreira^{a,*}, A.J. Goddard^b, O.C. Monteiro^a

^a Centro de Química e Bioquímica, Faculdade de Ciências, Universidade de Lisboa, Campo Grande, 1749-016 Lisboa, Portugal

^b Department of Chemistry, University of Leicester, Leicester LE1 7RH, UK

ARTICLE INFO

Article history:

Received 4 December 2017

Received in revised form 23 February 2018

Accepted 23 February 2018

Available online 24 February 2018

Keywords:

Cotton fibers

Semiconductor nanoparticles

Bismuthoxychloride

Titanium dioxide

Photocatalysis

Pollutants removal

ABSTRACT

The successful attachment of semiconducting BiOCl and TiO₂ nanoparticles to cotton fibers by *in situ* approaches is reported. The influence of the experimental conditions required for both Cotton-NPs preparation was investigated, namely the effect of the temperature required for TiO₂ synthesis. A homogeneous, continuous and stable TiO₂ layer, coating the fibers surface, was achieved, whereas BiOCl particles were found distributed on the fiber surface. The properties conferred upon NPs immobilization were evaluated considering morphological, structural and optical aspects as well as the photocatalytic ability granted by the nanoparticles, by means of microscopic and spectroscopic techniques (SEM, TEM, XRD and UV-vis). The functionalization with NPs conferred catalytic activity to the new materials, in the naphthol blue black (NBB) photodegradation, involving distinct oxidant species participation. The synthesis under mild conditions, at room temperature, the stability and the extended light absorption to the visible range of BiOCl when exposed to UV-vis light irradiation confers further advantage to the Cot-BiOCl sample as compared to the Cot-TiO₂. However, the extended reusability of the Cot-TiO₂ modified fibers imparts significant advantage to this material. Nevertheless, both modified fiber materials show promising potential applicability for photocatalysis and self-cleaning purposes.

© 2018 Elsevier B.V. All rights reserved.

1. Introduction

The functionalization of textile fibers to tailoring materials with specific properties is highly desirable and has been subject of intense research in recent years, with more than 740 papers published since 2010 regarding nanoparticles (NPs) and textile fibers (source: Web of Science, 01/2018). These innovative modified fibers have been used in a wide range of applications, namely medical, automotive and construction industries, and smart wearable systems [1–5]. Those materials take advantage from the natural fiber properties (e.g. abundance and renewal resources, low cost, biocompatibility and flexibility for processing) [6] and the ones well known from other materials such as nanoparticles, when synergistically combined [5,7].

Several approaches have been used for fibers modification with nanoparticles, such as immobilization of pre-synthesized NPs or one-pot approaches with *in situ* synthesis of NPs in the presence of

fibers [8–16]. To improve the NPs attachment and stability of the resulting materials, the fibers can be used both pristine or pre-modified [8–13]. The pre-modification can include for example thermal esterification, plasma treatment and silanization [15,17,18]. These treatments aim to create surface functionalities, e.g. carboxylic, hydroxyl, amine and thiol groups, to improve the interaction between fibers and the precursors and/or attached (nano)materials. For example, the esterification of cellulosic fibers using citric acid creates carboxylic acid groups and improves the attached TiO₂ content; plasma treatment of nylon introduces functional groups enabling the attachment of TiO₂ by electrostatic interaction between the slightly positive Ti⁴⁺ and the negative surface groups (–COO^{2–}, –O–O^{2–}); silanization results in the formation of a siloxane bridge with the fiber, allows the functionalization of the fibers by introducing free functional groups at the silane/air interface and acts as a surface coating conferring improved tensile properties [15,17,18].

The evaluation of the mechanical properties of the fibers, such as tensile strength and elongation at break, have been used to assess the effect of the modification imparted, both by pre-treatment and NPs attachment, which may affect those properties playing an

* Corresponding author.

E-mail address: vcferreira@fc.ul.pt (V.C. Ferreira).

important role on the fibers stability and durability [19–21]. For example, cotton fabrics treated with TiO_2 , ZnO and Ag-NPs show distinct mechanical properties before and after treatment. Lam *et al.* [19] showed that modification with TiO_2 NPs negatively affected the tensile properties, whereas the plasma pre-treatment improved the tensile strength of TiO_2 -modified samples, but regarding other properties a detrimental effect was observed. The coating with ZnO NPs was found to reduce the tensile strength of the cotton, supporting the findings that chemical finishes may reduce the tensile strength of cotton fabrics [20]. The sonochemical coating of textile fibers with Ag NPs also imparted a small loss of mechanical properties after modification [21].

Nanoparticles, such as Ag, Cu_2O , ZnO, TiO_2 , Bi_2WO_6 and magnetite, have been successfully attached to the fibers, conferring them enhanced properties, for example for magnetic, supercapacitor, UV protection, wettability and self-cleaning, antibacterial/antimicrobial and photocatalysis applications [16,18–27]. Of those, titanium dioxide (TiO_2) has attracted intense research interest due to its properties [8,11,12,15,22]. It is widely used in paper, leather and ceramics industry, in solar cells and in photocatalysis [15,28–30,33]. It can be found in three different crystalline forms, *rutile*, *anatase* and *brookite* and the relative proportion of each phase can be controlled during synthesis through the experimental conditions [28,30–33]. The *anatase* and *rutile* phases have been extensively investigated for technological applications such as photocatalysis since those are the phases with higher stability and activity due to lower recombination rate [30,31,34,35]. TiO_2 is commonly synthesized under hydrothermal methods at high temperature or when prepared at room temperature it requires further thermal treatment at high temperature (350–850 °C) and extended periods of time (4–16 h). The synthesis yields crystalline nanoparticles with size ranging from 5 to 32 nm, displaying tunable surface area (10.7 to 210 $\text{m}^2 \text{g}^{-1}$), band gap energy of about 3.2 to 3.3 eV and indirect transition semiconducting properties [30,32,36–39].

More recently, bismuthoxychloride (BiOCl) has also attracted significant interest due to its semiconducting properties, easy preparation, possibility of tuning its morphology and sensitization. BiOCl nanoparticles can be prepared by hydrothermal methods but recently some synthetic approaches performed at room temperature have also been reported [40–43]. These NPs show a preferential sheet like morphology due to its layered structure, which size and surface structure can be tailored by controlling the synthesis conditions. The sheet like particles can aggregate in flower-like hierarchical architectures; present surface area ranging from 5.4 to 74 $\text{m}^2 \text{g}^{-1}$, band gap energy between 2.25 and 3.5 eV and have been described as indirect transition semiconductors [43–48]. As TiO_2 , BiOCl has been frequently used for photocatalytic degradation of pollutants such as pharmaceuticals and personal care products (PPCPs) and industrial dyes under UV and/or visible light irradiation [43,45,46,49,50].

In what concerns the photocatalytic applications, the immobilization of the active nanoparticulate materials is frequently aimed regarding its recovery after use, to avoid its release to the environment, and/or to allow its reutilization. Therefore, finding suitable substrates for the stable immobilization of nanomaterials onto surfaces preserving its properties is of utmost importance.

Even though it has not been reported in the literature the immobilization of BiOCl on textile fibers, cotton fibers modified with TiO_2 have shown interesting results towards the development of self-cleaning, anti-bacterial, controlled wettability and photocatalytic materials [8,11–13]. These materials can be prepared both by dip-pad-dry-cure and *in situ* methods. The first using pre-synthesised TiO_2 NPs which is time consuming and may result in poor adhesion to the fiber surface [11]. The second, by hydrothermal treatment, for example after $\text{Ti}(\text{O}i\text{Bu})_4$ impregnation, has shown reusability problems after 3 cycles with efficiency loss

recognised by the authors [13]. Nevertheless, the cotton- TiO_2 materials have shown good photocatalytic response towards methyl orange, remazol brilliant blue R, cibacron blue F-R, neolan blue 2G and red wine and coffee stains under visible and sunlight irradiation [8,12,13].

In this work, the possibility of stable attachment of semiconductor nanoparticles displaying photocatalytic activity towards the degradation of pollutants and its properties conservation upon immobilization to a solid surface is investigated. This aims to contribute to the development of straightforward approaches for the preparation of modified textile fibers, such as cotton, displaying the so-called self-cleaning properties as well as the possibility to behave as environmentally-smart textiles with the ability to remove pollutants from the environment when exposed to light. Titanium dioxide in the *anatase* phase (TiO_2) and bismuthoxychloride (BiOCl) nanoparticles, deposited *in situ* on the surface of cotton fibers were prepared. The TiO_2 -modified cotton was used mainly for comparison purposes since TiO_2 is commonly regarded as a reference and one of the most studied photoactive materials, and has been widely used for photodegradation of dyes and other pollutants. To the best of our knowledge, this was the first time that BiOCl NPs were used for fiber modification as well as the successful and stable attachment of these NPs in a one-pot, room temperature *in situ* approach. The resulting materials structure and properties were analyzed and the photocatalytic activity and reusability of the samples tested towards the naphthol blue black di-azo dye. Naphthol blue black dye (NBB), is an azo compound commonly used in the textile industry. Encouraging photocatalytic responses for the photodegradation of this pollutant under UV and solar light irradiation were obtained using tridoped titania decorated on oxidized multiwalled carbon nanotubes ($\text{Gd,N,S-TiO}_2/\text{MWCNT}$), CeO_2 , CeMnO_2 , CeSnO_2 and TiO_2 [51–54].

Further insight into the photodegradation processes involving the studied catalysts, was achieved by using terephthalic acid (TA), allowing the detection of hydroxyl radicals formation, and benzoquinone (BQ), as scavenger for superoxide radicals.

2. Materials and methods

2.1. Chemicals and synthesis

All chemicals were analytical grade and used as received without further purification. All solutions were prepared with distilled water. Commercial TiO_2 nanoparticles (Degussa, P25, here denoted TiO_2 P25) were used as received and only for comparison purposes as a standard TiO_2 material.

Cotton fibers were commercially available, Águia, Coast®, 100% cotton, tread nr. 6. Prior to the surface modification of cotton fibers with nanoparticles, propan-2-ol (IPA) was used for washing them for 5 min at room temperature, after which they were dried in the oven at 50 °C and stored before use; the IPA washed fiber are designated Cotton-IPA. Considering that the attachment of NPs to the surface of fibers by *in situ* approach benefits from a successful impregnation of the reactants within the fibers structure, the use of solvents such as propan-2-ol is beneficial [55]. Propan-2-ol is well known to decrease the activation energy in cotton fibers which is related to the energy necessary to disrupt the intermolecular forces in the internal structure of the fiber allowing, for example, dye penetration. This has a similar effect to that reported by Emam *et al.* [16] in which the pre-treatment of cotton fabric by alkalization, besides activating the cellulose macro-molecules, also swells the fabrics facilitating the impregnation of reactants prior to the deposition step and resulting in higher content of attached NPs than on untreated fibers.

2.1.1. Modification of cotton fibers with nanoparticles

The modification of cotton fibers with bismuth oxychloride (BiOCl) nanoparticles was performed by immersing the fibers (0.3 g) for 5 min, under stirring, in 25 mL of a 20 mM BiCl₃ in HCl acidic solution (to ensure complete dissolution of BiCl₃) allowing cotton fibers impregnation with BiCl₃, after which 100 mL of H₂O were added. The decrease in pH induced the formation of BiOCl nanoparticles. The mixture was kept under stirring overnight at room temperature. After synthesis, the modified cotton fibers were washed three times with distilled water, dried in the oven at 50 °C and stored.

The synthesis of TiO₂ was performed as previously described in the literature in a two-step methodology: (1) synthesis of an amorphous precursor at room temperature and (2) hydrothermal synthesis [56,57]. Briefly, the amorphous titanium oxide precursor was prepared by dilution in a 1:2 ratio of a titanium trichloride solution (20 wt.-% in 20–30 wt.-% HCl, Aldrich) in 2 M HCl. To this solution, a 4 M ammonium solution was added dropwise under vigorous stirring, until complete precipitation of a white solid. The suspension was allowed to rest overnight at room temperature, filtered, rinsed three times with distilled water, and then collected by filtration. The final solid was stored wet. The amorphous nature of the solid precursor obtained by this synthesis route, with a Ti:O ratio of 1:4, has been previously characterized and reported [57]. The TiO₂ particles were then synthesized at 160 °C for 24 h in an autoclave using 6 g of wet precursor in 55 mL of H₂O (pH 7.3 suspension) and 1.5 g of cotton fibers (pH of solution ≈ 6.5). After synthesis, the modified cotton fibers were washed three times with distilled water, dried in the oven at 50 °C and stored.

The cotton fibers modified with TiO₂ and BiOCl NPs are designated by Cot-TiO₂ and Cot-BiOCl, respectively.

Pure TiO₂ and BiOCl nanoparticles were also prepared without fibers using the same procedures described above. The particles in suspension were separated by centrifugation, washed three times with distilled water, dried in the oven at 50 °C and stored.

2.2. Characterization

X-ray powder diffraction (XRD) analysis was performed using a Philips X-ray diffractometer (PW 1730) with automatic data acquisition (APD Philips v3.6B), using Cu K α radiation ($\lambda = 0.15406$ nm) and working at 40 kV/30 mA. The diffraction patterns were collected in the range $2\theta = 7\text{--}70^\circ$ with a 0.02° step size and an acquisition time of 2.0 s per step. Thermogravimetric analysis (TGA) was performed in a Perkin-Elmer TGA7 Thermogravimetric Analyzer using ca. 10 mg of sample and a heating rate of $10^\circ\text{C min}^{-1}$. All measurements were performed in air. Optical characterization of the powder samples was carried out by UV–vis diffuse reflectance (DRS) using a Shimadzu UV-2600PC spectrophotometer, using an ISR 2600plus integration sphere. The DRS spectra were recorded in the wavelength range of 200–1400 nm. Infrared spectroscopy with Fourier transform (FTIR), was performed in a Nicolet 6700 FT-IR spectrophotometer. The FTIR spectra were collected in transmittance mode using KBr pellets containing the sample, in the spectral interval between 400 and 4000 cm^{-1} with accumulation of 128 spectra per measurement. Transmission electron microscopy (TEM) was carried out using a JEOL 200CX microscope operating at 200 kV and scanning electron microscopy (SEM) in a field emission gun – scanning electron microscope JEOL-7001F (FEG-SEM), operating at 5 kV. Specific surface area was estimated by the Brunauer-Emmett-Teller (B.E.T.) method, from nitrogen (Air Liquide, 99.999%) adsorption data at -196°C , using a volumetric apparatus from Quantachrome mod. NOVA 2200e. The samples, weighing about 100 mg, were previously degassed for 2.5 h at 150°C at a pressure lower than 0.133 Pa. The tensile

strength of the fibers was obtained using an Instron 3343 tensiometer, with propriety Bluehill software version 2.0. A 500 N load cell was utilised for the tests with the crosshead speed of 10 mm/min. All samples were characterised at least in triplicates for statistical analysis. All samples were characterised at least in triplicates for statistical analysis. UV–vis spectroscopy of liquid samples was performed in the same spectrophotometer described above (Shimadzu UV-2600PC) using quartz cuvettes with 1 cm optical path. The spectra were collected in the interval between 200 and 900 nm. Fluorescence spectroscopy was performed in a Spex Fluorolog 3–22/Tau 3 fluorescence spectrophotometer. The excitation was performed at 315 nm and the emission at 425 nm and the spectra collected in the intervals from 250 to 400 nm (Ex.) and 320 to 575 nm (Em.). The electrochemical characterization was performed using a CH Instruments (CHI 600) potentiostat, in a 3-electrode/2-compartment configuration, by cyclic voltammetry at 50 mV s^{-1} . The reference, counter and working electrodes were saturated calomel (SCE), platinum foil and platinum disc, respectively. The dye solution was prepared by dissolving NBB in a 0.1 M LiClO₄ solution in acetonitrile.

2.3. Photocatalytic activity

All photocatalytic experiments were conducted using the procedure described elsewhere [48,58]. A 450 W Hanovia medium pressure mercury-vapor lamp was used as radiation source in a 250 mL refrigerated photoreactor. The total irradiated energy was 40–48% in the ultraviolet range and 40–43% in the visible region of the electromagnetic spectrum. Prior to irradiation, 250 mg of sample – Cot-NPs – (20 mg if using pure NPs) were suspended in 150 mL of a naphthol blue black (NBB) solution (10 ppm) and were stirred in dark conditions for 60 min to allow the adsorption/desorption equilibrium. After this time an aliquot of solution was collected to evaluate the adsorption of NBB on the catalyst and used as $t=0$ for the photocatalytic degradation. During irradiation, aliquots of the suspensions were collected at regular intervals using a peristaltic pump, centrifuged and analyzed by UV–vis spectroscopy. The same procedure was used in the presence of 1,4-benzoquinone (1 mM). The amount of powder used, 0.13 g L^{-1} , was selected according to the following parameters: (1) successful use in studies previously performed and being within the range reported in literature [48,54,58] (allowing the comparison with other catalysts performance and dyes photodegradation) and (2) achieving complete removal of the pollutants under study within the typical experimental time scale used, ≤ 2 h, under UV–vis irradiation. The amount of modified fibers was selected based on the second parameter above, to ensure that the complete removal of the pollutant was reached, at least for the materials displaying better performance.

The re-utilization studies were performed using the experimental conditions described above and aliquots were collected at $t=0$ and $t=30$ min (maximum irradiation time used). The procedure was repeated 6 times between which the Cot-NPs samples were removed from the previous solution, washed with water, the excess of water removed by absorption in absorbing paper and transferred to a fresh NBB solution. The BiOCl sample was recovered by centrifugation, washed with water and transferred, wet, to a fresh NBB solution.

The terephthalic (TA) acid degradation study was performed in a similar way, using 10 mg of photocatalyst and 150 mL of a 3 mM TA prepared in 10 mM NaOH solution and using a dark period of 30 min. The TA photodegradation was evaluated by fluorescence analysis of the 2-hydroxyterephthalic acid (2-HTA) in the collected aliquots.

3. Results and discussion

3.1. Structural and morphological characterization

After modification, the nanoparticles-coated cotton fibers were characterized by XRD. In Fig. 1 are the diffractograms obtained from which it is clearly noticed the presence of TiO_2 and BiOCl NPs attached to the fibers. The diffraction peaks at 25.28° , 37.80° , 48.05° , 53.89° and 55.06° for Cot- TiO_2 (Fig. 1a) are assigned to the TiO_2 anatase phase (ICDD PDF4 file: 21–1272) and the peaks namely at 12.00° , 25.88° , 32.52° , 33.47° , 36.54° , 49.72° , and 55.11° for Cot- BiOCl (Fig. 1b) correspond to crystalline BiOCl (ICDD PDF4 file: 01–085–0861) [48]. Additionally, the crystalline nature of the cotton fibers is observed in the diffractograms obtained for the pristine fiber with peaks at 14.96° , 16.68° , 22.94° and 34.53° , in agreement with those reported in literature [10].

The treatment of cotton fibers at 160°C for 24 h was necessary to the *in situ* modification with TiO_2 by the hydrothermal method. This did not produce any significant change or damage in the cotton fibers as shown by XRD, DRS, FTIR and TG analyses performed before and after exposure of pristine fibers to those conditions in the absence of TiO_2 precursor (Fig. S1). The thermogravimetric analysis of the pristine fibers (Fig. S1d) allows to confirm that those are stable up to $ca. 260^\circ\text{C}$ and that the modification with TiO_2 at 160°C should not cause any damage on them. This was further corroborated after exposure of pure cotton fibers aqueous suspension to $160^\circ\text{C}/24\text{ h}$, without TiO_2 precursor,

with only a small decrease on the decomposition temperature observed ($ca. 23^\circ\text{C}$).

The effect of the immersion in acidic solution on the cotton properties, during the impregnation prior to BiOCl synthesis, was also considered. The analysis of the unmodified cotton fibers before and after immersion in a HCl 1 M solution for 24 h (Fig. S1) show no changes in the XRD, FTIR and DRS data, indicating that the immersion of the cotton fibers in the BiCl_3 acidic solution for the impregnation time (5 min) should not induce any damage to the fibers. On the TG analyses of pure cotton fibers before and after immersion, included in Fig. S1d, only a small decrease in the thermal decomposition temperature was observed ($ca. 34.5^\circ\text{C}$).

Furthermore, the tensile properties analysis data depicted in Table 1, show that, once washed with propan-2-ol, Cotton-IPA, the tensile strength decreases by about 9 and 6% and the Young's modulus by 4 and 5% for Cot- BiOCl and Cot- TiO_2 samples, respectively, confirming the small impact of the modification conditions on the fiber properties. Those changes are within acceptable range for cotton and therefore it can be concluded that the procedure applied for the fibers modification did not cause any significant damage to its structure [21]. It is worth mentioning that the impact of washing the fibers with propan-2-ol results in a 20% stiffness decrease (Young's modulus decreases from 1135 to 873 MPa upon washing the Cotton fibers), corroborating the decrease in activation energy which facilitates the reactants impregnation (see Section 2.1) [16,55]. In addition, the impact of washing with propan-2-ol on the tensile strength was found to be very small, only 1% decrease, from 220.1 MPa for pristine Cotton fibers to 217.9 MPa for Cotton-IPA, and without significant impact on the fibers properties.

Although the modification of cotton fibers with TiO_2 has been previously reported [8,9,11,13], to our knowledge, this is the first time it has been successfully attempted with BiOCl nanoparticles.

The morphological characterization was achieved by SEM analyses for the pure BiOCl and TiO_2 nanoparticles and the Cot- BiOCl and Cot- TiO_2 modified fibers, as illustrated in Fig. 2. Due to their size, the pure BiOCl particles were analysed by SEM, and present an irregular plate-like morphology with size ranging from 0.12 to $3.13\text{ }\mu\text{m}$ (average $1.0 \pm 0.4\text{ }\mu\text{m}$) and thickness from 58 to 575 nm, as shown in the SEM image presented in Fig. 2. For the Cot- BiOCl sample, the BiOCl plates are distributed on top of the cotton surface (Fig. 2 – bottom panel), some aggregated, and its presence has also been confirmed by EDS analysis (Fig. 3). The increased contrast obtained by using backscattered electrons (Fig. 2 – bottom panel, right) unveils the cotton surface area with higher concentration of BiOCl NPs. The SEM analysis of the TiO_2 NPs, prepared in the absence of fibers, shows aggregated NPs in Fig. 2 (top panel), which typical TEM image is also depicted in the inset included in the figure. These have an average size of $12 \pm 2\text{ nm}$ (particles size measured using the Image J software, National Institute of Health), which agrees with the crystallites size (10 nm) estimated from XRD data using the Scherrer equation. In the case of cotton modification with TiO_2 , the presence of the NPs was confirmed by the detection of a globular-like morphology on top of the fibers surface (Fig. 2 – middle panel) and has also been corroborated by EDS analysis shown in Fig. 3. The virtually continuous and uniform TiO_2 film is formed by small TiO_2 aggregates with sizes between 50 and 100 nm (Fig. 2 – middle panel, right), resembling the morphology observed in the SEM image of pure TiO_2 NPs (Fig. 2 – top panel).

By using backscattered electrons to image the surface (Fig. 2, bottom panel, middle image), it was possible to distinguish areas with higher density of BiOCl composed of flower-like aggregates in agreement with the reported in the literature for these materials [40,45,48,59]. It is worth mentioning that an excess of TiO_2 and BiOCl NPs in suspension was obtained after synthesis suggesting

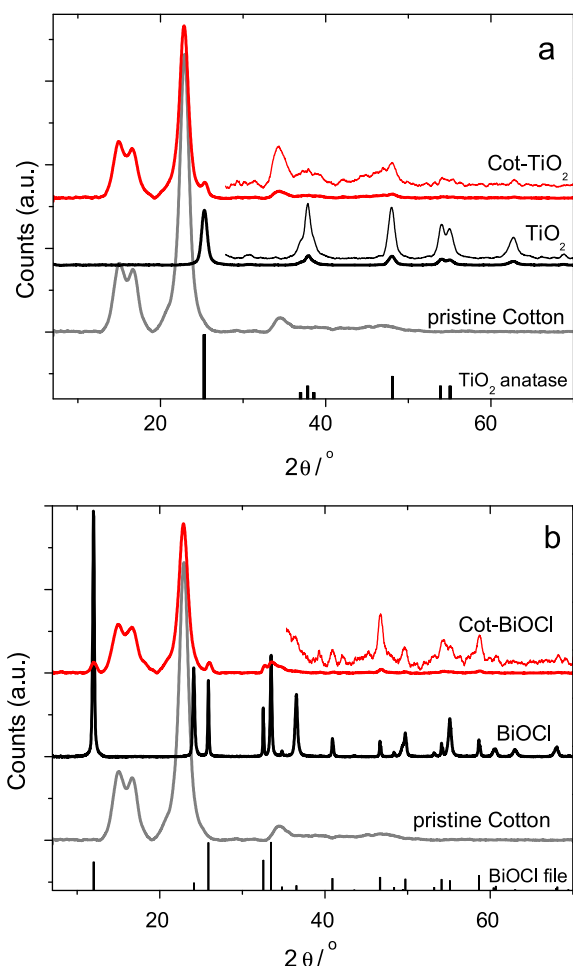
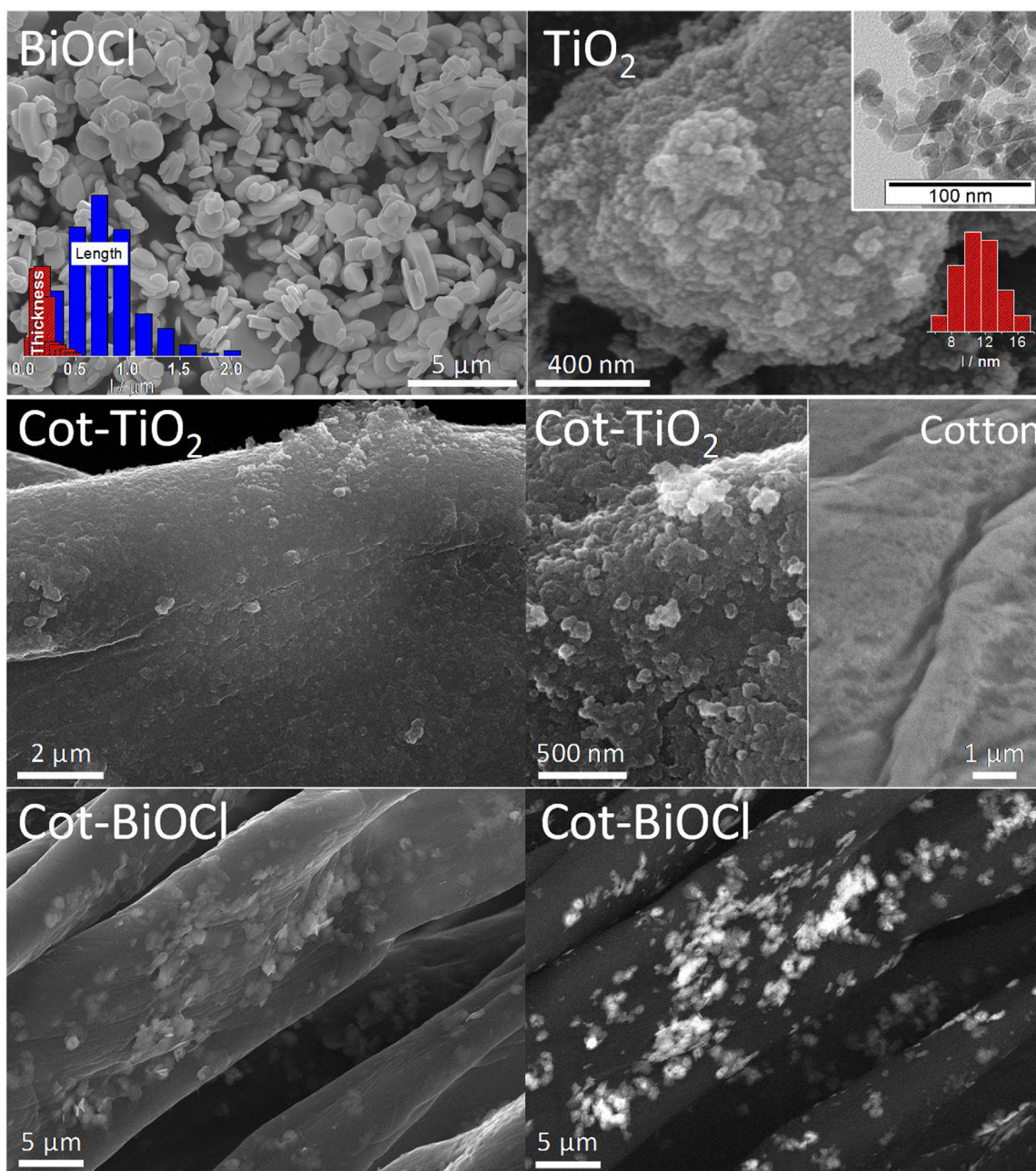


Fig. 1. XRD patterns for cotton fibers modified with TiO_2 (a) and BiOCl nanoparticles (b), and comparison with pure TiO_2 , BiOCl and pristine cotton fibers. Included in figures are amplified diffractogram details.

Table 1Tensile properties of pristine cotton fibers, before and after washing with propan-2-ol, and modified fibers with BiOCl and with TiO₂ nanoparticles.

Sample	d/mm	Tensile strength /MPa	% change	Young's Modulus /GPa	% change
Cotton	0.50	220.1	—	1.1347	—
Cotton-IPA		217.9	−1.0	0.9083	−20.0
Cot-BiOCl	0.50	197.7	−9.3*	0.8728	−3.9*
Cot-TiO ₂		204.8	−6.0*	0.8614	−5.2*

* Using Cotton-IPA as reference.

**Fig. 2.** SEM images for pure TiO₂ and BiOCl (top panel), modified cotton fibers Cot-TiO₂ (middle panel) and Cot-BiOCl (bottom panel) and comparison with pristine cotton (middle panel, right). Inset in top panel: TEM image of pure TiO₂ NPs and size distribution charts for pure BiOCl (length and thickness) and TiO₂ NPs. All SEM images have been obtained using secondary electrons, except for Cot-BiOCl right image obtained with backscattered electrons.

that the surface saturation was likely to have been achieved under the experimental conditions used. However, it can be anticipated that by control of the fiber to precursor (Cot-TiO₂) and fiber to BiCl₃ (Cot-BiOCl) ratios, the degree of coverage can be adjusted as it has

been reported for silica spheres decorated with zinc sulphide NPs [60]. It is noteworthy that both NPs-coated fibers have been largely handled after modification and before morphologically characterized by SEM. The practical absence of damage on the NPs coating

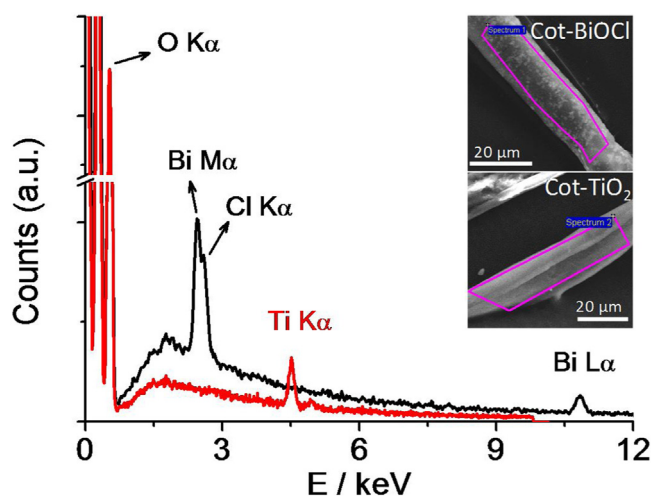


Fig. 3. EDS spectra of Cot-TiO₂ and Cot-BiOCl samples.

layer suggests that they present a high degree of stability and flexibility and do not easily break upon manipulation, which is by itself an advantage.

The surface area of the modified fibers, obtained by nitrogen adsorption isotherm through the B.E.T. method, (Table 2) show that, upon modification with TiO₂ there is an increase in the surface area of the fibers. The surface area of the Cot-TiO₂ increases almost two-fold (77%) reflecting the high surface area of the small NPs (89.730 m² g^{−1}) as compared with that of pristine cotton (5.655 m² g^{−1}). This result seems to corroborate the existence of a uniform, continuous and smooth layer of NPs on top of the cotton fibers surface. Whereas the assembly of plate-like BiOCl NPs in a preferential flat orientation on the surface results in only 24% increase of surface area for Cot-BiOCl (7.034 m² g^{−1}).

3.2. Optical characterization

In Fig. 4 are represented, for the prepared materials, the Kubelka–Munk function plots, F_{KM} , which are related to the diffuse reflectance, R , through the equation [48,61]:

$$F_{KM}(R) = (1 - R)^2 / 2R \quad (1)$$

F_{KM}

in situ

The optical band gap energy, E_g , of the modified fibers was estimated from the Tauc plot for indirect transitions:

$$(F_{KM} h\nu)^{1/2} \text{ vs } h\nu \quad (2)$$

where h is the Planck constant and ν is the frequency, by extrapolation of the linear part of the curve close to the band edge to zero absorption (Fig. 4). The results obtained are included in Table 2, from which can be retrieved that the absorption edge of BiOCl is about 0.2 eV higher than that of TiO₂. The NPs modified fibers show an E_g shift towards higher energy of about 0.1 eV which

is probably due to the quantum confinement effects on the smaller size particles when grown on the fibers surface.

3.2.1. Adsorption studies

Naphthol blue black or naphthol acid 1 is an acid dye, a di-azo compound, with the structure illustrated in Scheme 1. This dye was selected for the photodegradation studies due to two main reasons. First, NBB is a commonly used dye in textile industry and therefore studies regarding its swift and efficient removal and/or degradation from waste waters are of utmost importance. Secondly, to better understand the photocatalytic process, the absence and/or low adsorption of the dye on the catalyst surface is an advantage, eliminating the dye sensitization which frequently masks the pure catalyst contribution to the photocatalytic response leading to erroneous interpretation of the experimental data [40,62]. Good examples are those in which materials are adequate catalysts towards dye degradation upon visible light illumination when its band gap energy is in the UV range.

Under the experimental conditions used, NBB exhibited low adsorption on the NPs surface as the graph in Fig. 5 clearly shows. In the presence of fibers, the amount of adsorbed dye may be underestimated due to water absorption by cotton, however no significant adsorption was observed for NBB (Fig. S2), decreasing the possibility of erroneous interpretation due to dye removal by adsorption on the fibers.

For Cot-BiOCl and Cot-TiO₂, values of 0 and 5.3% were correspondingly obtained, reflecting the slightly higher adsorption ability of TiO₂ as compared with BiOCl. This, however, is not directly reflected by the NPs surface area difference, since pure TiO₂ possesses a surface area 10 times higher than pure BiOCl whereas the percentage of adsorbed NBB is only 5-fold (14.3 and 2.7% for pure TiO₂ and BiOCl, respectively).

The pH of a NBB solution is about 6.7 and BiOCl is known to have a potential of zero charge (p.z.c.) of 4.5 and for TiO₂ p.z.c. values between 6.3 and 6.6 have been reported [48,49,63,64]. On the other hand, the complexity of the NBB molecule and the absence of information on its pK_a, makes difficult the prediction of NBB structural state in the pH of the solution used.

However, in the NBB solution, the catalysts have a negatively charged surface and the dye does not adsorb (or at least not significantly) on the surface, most probably due to repulsive interactions, indicating that at pH 6.7 NBB is in the anionic state with deprotonated sulphonate groups. It is the higher p.z.c. of TiO₂ NPs together with the surface area (6.3–6.6 and 89.7 m² g^{−1}), as compared to that of BiOCl NPs (4.5 and 8.8 m² g^{−1}), that are responsible for the increased NBB adsorption in the former material. Moreover, the very low p.z.c. of cellulose fibers (p.z.c. ≤ 2.5 [65]) clearly explains the poor adsorption of NBB on the cotton fibers surface.

3.2.2. Naphthol blue black photodegradation studies

The NBB photodegradation was monitored by means of UV–vis spectroscopy from the absorption band intensity of the peak at 618 nm. In Fig. 6a are the UV–vis spectra obtained during the dye photodegradation under UV–vis radiation, using Cot-BiOCl as catalyst. For all the experiments, the 618 nm peak intensity decreases with irradiation time and after 15 min the NBB has been completely removed from the solution using Cot-TiO₂ whereas a slightly slower process was observed for Cot-BiOCl, which required about 20 min to complete the process (Fig. 6b). However, when using pure TiO₂ and BiOCl NPs, the later displays a much better catalytic response with the complete NBB degradation after 7 min of irradiation, whereas TiO₂ takes about 12 to 15 min to complete the process (Fig. S3). Additionally, commercial TiO₂ P25 nanoparticles were used as a standard material. These are composed by a mixture of rutile and anatase phases known as advantageous

Table 2

Surface area, $A_{B.E.T.}$, and optical band gap energy, E_g , for pristine cotton fiber, pure TiO₂ and BiOCl NPs and Cot-TiO₂ and Cot-BiOCl samples.

Sample	$A_{B.E.T.}/m^2 g^{-1}$	E_g/eV
Cotton	5.655	—
TiO ₂	89.730	3.14
BiOCl	8.848	3.35
Cot-TiO ₂	10.022	3.23
Cot-BiOCl	7.034	3.45

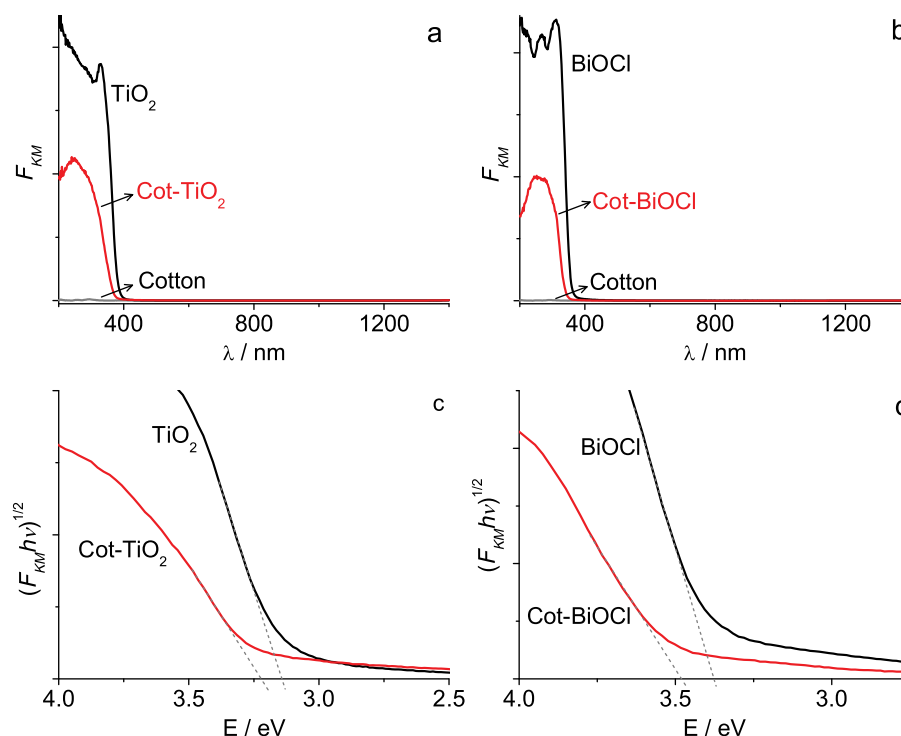
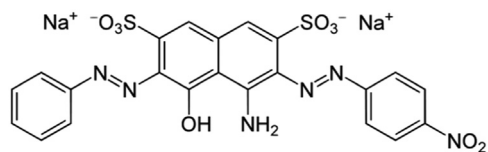


Fig. 4. Diffuse reflectance spectra for (a) Cot-TiO₂ and (b) Cot-BiOCl, and comparison with pure TiO₂ and BiOCl nanoparticles and pristine cotton fibers. (c and d) corresponding Tauc plots for the synthesized samples for indirect transitions.



Scheme 1. Naphthol blue black structure.

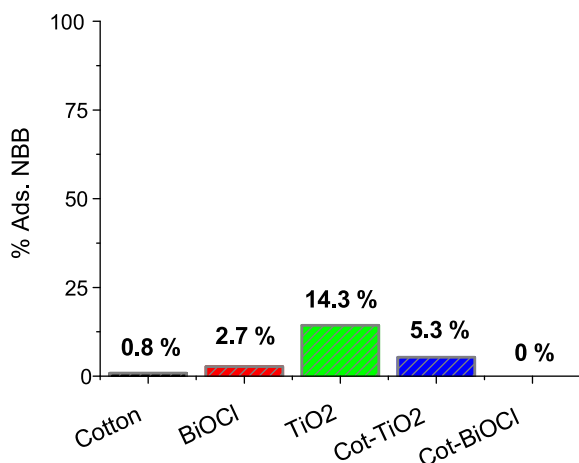


Fig. 5. Amount of adsorbed NBB on the surface of pristine cotton, pure TiO₂ and BiOCl NPs, and Cot-TiO₂ and Cot-BiOCl samples.

regarding the efficiency of electron–hole recombination in the presence of both crystals phases [66]. By using the P25 NPs it took 30 min to completely remove the dye from the solution (Fig. S3). This is most probably due to the lower surface area of the P25 NPs as compared with those synthesized in this work (28.376 and $89.730 \text{ m}^2 \text{ g}^{-1}$, respectively). This also suggests that, although high

efficiency was expected to the P25 NPs, in this case, to the same amount of catalyst used and comparable band gap energy of the P25 and the synthesized TiO₂ NPs (3.02 vs 3.14 eV, respectively), it was the surface area the main factor affecting the photocatalytic response.

It is worth mentioning that the cotton fibers do not interfere with the photodegradation process; the NBB photodegradation is unaltered in the presence and absence of the cotton fibers (Fig. 6b) and a response comparable to the pure photolysis (photodegradation due to light irradiation only, in the absence of catalyst) is observed, with near 50% degradation. At the end of the photodegradation experiments, the remaining absorption band at 266 nm, can be assigned to NBB degradation products, most likely to molecules containing an aromatic ring as previously reported for RhB photocatalytic degradation [48]. The full identification of the degradation products was not the aim of this work and will require a more detailed investigation using GC–MS and/or HPLC, which will be subject of a future publication.

3.2.3. Reusability studies

The Cot-BiOCl and Cot-TiO₂ samples have been submitted to six reutilization cycles (Fig. 7). The Cot-TiO₂ sample showed to be remarkably stable under the experimental conditions used here with about $99 \pm 1\%$ removal efficiency. This represents an advance as compared with other studies reported in the literature, in which efficiency loss is observed already after the 1st cycle [13]. In the case of Cot-BiOCl, the high efficiency was maintained up to 4 cycles ($97 \pm 2\%$), after which a decrease was observed to 86 and 70% for the following 2 cycles, respectively. At this point it could be speculated if the efficiency loss was due to catalyst loss or self-degradation.

In the event of mass loss occurring for the Cot-TiO₂ sample, the results seem to indicate that the overall active surface area is kept constant throughout at least 6 reutilization cycles. The photocatalytic process is mainly a surface-governed phenomenon, especially in the case of catalyst-coated substrates in which the

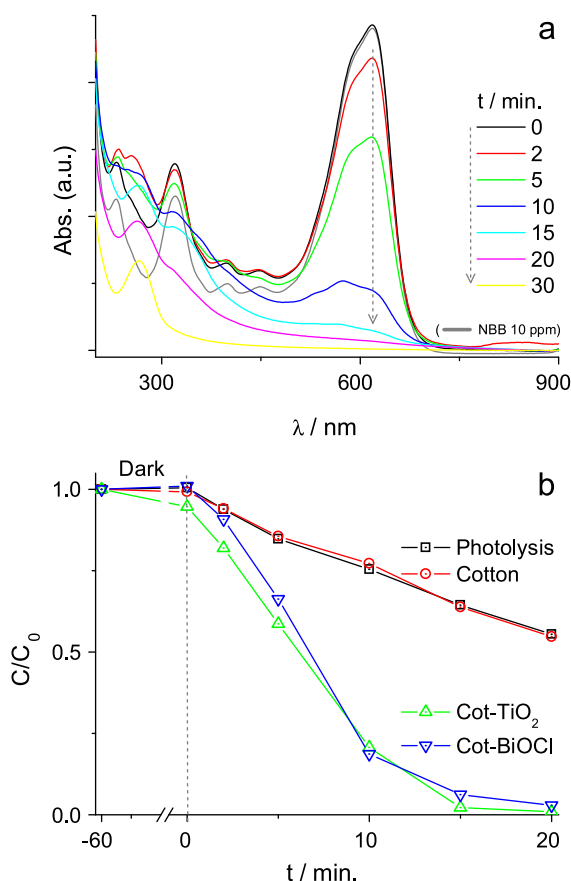


Fig. 6. (a) UV-vis spectra for the aliquots collected during the photodegradation of NBB using Cot-BiOCl as catalyst and (b) time profiles of adsorption and photocatalytic performance of Cot-TiO₂, Cot-BiOCl, Cotton and photolysis responses, for NBB degradation under UV-vis light irradiation after 1 h in the dark.

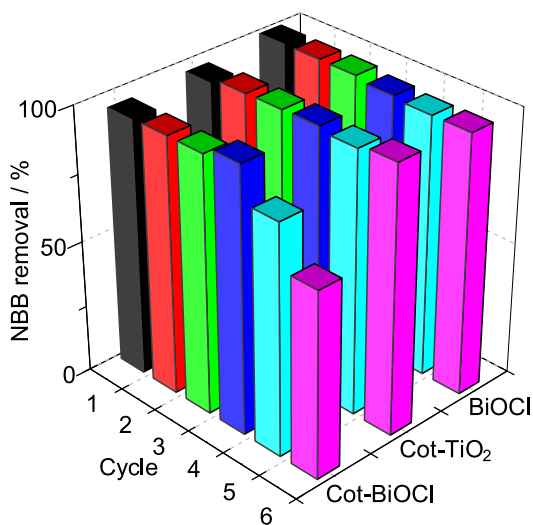


Fig. 7. Removal efficiency of NBB using the Cot-BiOCl and Cot-TiO₂ samples, and BiOCl nanoparticles, under 6 cycles of UV-vis irradiation.

buried part of the coating is less exposed to the radiation and less accessible to the dye molecules. SEM images after the 6 reutilization cycles do not allow any further insight (Fig. S4).

Regarding the Cot-BiOCl sample, in order to answer the question above, pure BiOCl was also used for reusability assays. The data obtained, depicted in Fig. 7, shows that no catalyst

degradation occurs during irradiation cycles since the efficiency was preserved throughout the experiments ($99 \pm 1\%$). Also, since the Cot-TiO₂ sample maintain its activity during the 6 reutilization cycles it seems that no self-degradation of the modified fibers occurs. Consequently, it can be assumed that, when using BiOCl supported on cotton fibers, the catalyst loss is the main factor responsible for the efficiency decrease after 4 cycles. This was further confirmed by SEM imaging (Fig. S4), through which a partial depletion of the catalyst could be detected on the cotton fiber surface as compared with the as-prepared sample (Fig. 3, bottom panel), and by surface area measurement, which decreased from $7.03 \text{ m}^2 \text{ g}^{-1}$ (Table 2) to $6.17 \text{ m}^2 \text{ g}^{-1}$ after the 6 reutilization cycles. Regardless of that, the dark coloration of the cotton fibers, imparted by the presence of BiOCl irradiated by UV-vis light (see below for further details), is clearly visible after 6 reutilizations (Fig. S5) agreeing with only a partial loss of catalyst.

3.2.4. Photocatalytic process evaluation studies

Considering the amount of removed dye from solution at $t = 10 \text{ min}$ (81% for Cot-BiOCl and 79% for Cot-TiO₂) and taking into account that Cot-TiO₂ has about 30% higher surface area than Cot-BiOCl, a better performance was attained with the material containing BiOCl. This indicates that the surface area of the catalyst is not the main parameter responsible for the sample response.

Regarding the band gap energy, Cot-TiO₂ presents a lower value (3.23 eV) as compared with Cot-BiOCl (3.45 eV), which does not by itself explain the observed photocatalytic results. Bearing this in mind, three approaches have been followed to gain further insight on the underlying parameters: (i) evaluation of the stability of the catalyst nanoparticles to UV-vis irradiation, (ii) determination of the band position in the energy scale for the catalysts and dye, and (iii) evaluation of the involvement of oxidant radicals on the photocatalytic performance through the degradation study of terephthalic acid and of NBB in the presence of 1,4-benzoquinone.

A fast BiOCl catalyst color change was detected after 2 min of exposure to the UV-vis radiation (Fig. S6), in agreement with a similar effect previously reported [67]. This fact results in a clear extension of the absorption to the whole visible range for BiOCl NPs reflecting the changes undergone by these particles, hereinafter referred as BiOCl_{UV}. No similar effect was found for TiO₂ (Fig. S7a). The decreases of the band gap energy of BiOCl_{UV} to $E_g \approx 0.60 \text{ eV}$ (Inset in Fig. S7a) can account to the photocatalytic performance of this material. Under the experimental conditions used, no degradation or transformation of the BiOCl catalyst was detected by XRD after irradiation. Only a crystallinity increase was observed most probably due to crystalline structure rearrangements induced by the exposure to high energy UV radiation (Fig. S7b).

In terms of energy, the valence (VB) and conduction (CB) bands energies, E_{VB} and E_{CB} , for these materials, included in Table 3, have been estimated according to that described in the literature:

$$E_{VB} = X - E^e + 0.5 E_g \quad (3)$$

Table 3

Estimated band energy position for pure BiOCl and TiO₂ and Cot-BiOCl and Cot-TiO₂ samples and HOMO and LUMO energy position for NBB.

Sample	χ	E_g/eV	V_B/eV	C_B/eV
BiOCl	6.36	3.35	3.54	0.19
BiOCl _{UV}		≈ 0.60	2.16	1.56
Cot-BiOCl		3.45	3.58	0.14
TiO ₂	5.81	3.14	2.88	-0.26
Cot-TiO ₂		3.23	2.92	-0.30

Dye	$\lambda_{\text{edge}}/\text{nm}$	E_g/eV	$E_{\text{onset red.}}/\text{V vs NHE}$	$E_{\text{HOMO}}/\text{eV}$	$E_{\text{LUMO}}/\text{eV}$
NBB	701	1.77	-0.185	1.96	0.18

For symbols refer to text.

and

$$E_{CB} = E_{VB} - E_g \quad (4)$$

assuming that the energy of free electrons, E^e , on the hydrogen scale is about 4.5 eV and the Pearson absolute electronegativity values, χ , are 5.81 and 6.36 eV for TiO_2 and BiOCl , respectively [48,68–70]. The NBB highest occupied molecular orbital (HOMO)–lowest unoccupied molecular orbital (LUMO) energy gap ($E_g = 1.77$ eV) was estimated through the absorption edge, λ_{onset} , in the UV–vis spectrum according to:

$$E_g = 1242/\lambda_{\text{onset}} \quad (5)$$

and the HOMO and LUMO energy levels, E_{HOMO} and E_{LUMO} , from the reduction onset potential ($E_{\text{onsetred}} = -0.185$ V vs NHE) obtained by cyclic voltammetry (Fig. S8), considering that [40,71,72]:

$$E_{\text{HOMO}} = E_{\text{LUMO}} + E_g \quad (6)$$

Based on the estimated values included in Table 3, the energy diagram depicted in Scheme 2, showing the relative band energy positions for TiO_2 , BiOCl , BiOCl_{UV} and NBB assists in the understanding of the photocatalytic process through the generation of active species that may be responsible for the catalytic response towards dye photodegradation.

To gain some insight into the involvement of the hydroxyl radical ($\cdot\text{OH}$) in the photocatalytic response of the materials, the pure catalysts TiO_2 and BiOCl have been used for the photodegradation of a probe molecule, the terephthalic acid (TA). The degradation of TA under UV–vis radiation was evaluated regarding the production of the fluorescent degradation product 2-hydroxyterephthalic acid (2-HTA). This enabled the evaluation of the impact of the formation of the $\cdot\text{OH}$ on the observed catalytic activity of the photoactive materials used [36,73]. Additionally, TA is also a compound of interest for photocatalytic degradation studies once it is widely used in the production of polymers and a well known contaminant with noxious health effects [73]. In Fig. 8 are illustrated the results obtained, from which the increase of the 2-HTA production with irradiation time is clearly observed for TiO_2 and BiOCl NPs.

The fluorescence signal stabilizes after 10 min of irradiation for TiO_2 most probably due to simultaneous consumption of 2-HTA in further degradation steps and production of other non-fluorescent products [73]. On the other hand, for BiOCl , a slower increase is observed in time, Fig. 8b. In this case, the production of 2-HTA is less than that observed for pure photolysis reaction (without catalyst) (Fig. 8c), indicating that BiOCl is not catalytic for the $\cdot\text{OH}$

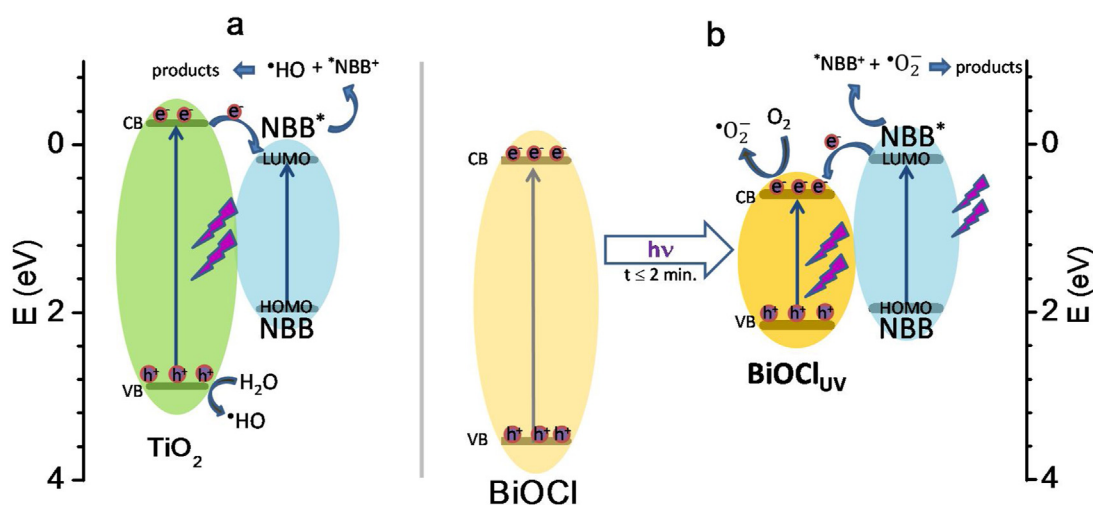
production. Therefore, this radical should not be the main active species involved in the degradation of NBB using this catalyst. Consequently, the high and similar activity displayed by both Cot-NPs materials for the photodegradation of the model di-azo dye NBB may involve different active species.

In fact, for TiO_2 the production of hydroxyl radicals has been frequently reported as the main responsible for its photocatalytic activity towards several pollutants degradation, for example to the non-adsorbing azo dye reactive red 195, sulfamethazine antibiotics and TA degradation [40,49,74]. In the case of BiOCl the superoxide radical ($\text{O}_2^{\cdot-}$) and holes (h^+) species have been more frequently involved in photodegradation reactions of rhodamine B and methyl orange compounds [40,67,75–78]. The photogenerated holes could directly oxidize organic molecules, however since NBB does not adsorb on the BiOCl catalyst surface (shown above) the direct oxidation by holes is not likely.

On the other hand, the oxygen vacancies on the surface of the BiOCl can behave as electron traps promoting the photogenerated electron-hole pairs separation [67,76,79,80]. Consequently, the electrons in the conduction band of BiOCl will promote the superoxide radical formation (Scheme 2). Considering the superoxide radical role, the impact of the presence of a superoxide scavenger on the photodegradation of NBB was evaluated using 1 mM of 1,4-benzoquinone (BQ). The presence of BQ completely inhibited the catalytic response of BiOCl , undoubtedly indicating that is the superoxide radical the main active species responsible for the photocatalytic performance of BiOCl and Cot- BiOCl samples (Fig. 9).

The small increase in the absorbance signal at the beginning of the irradiation is due to the difficulty in estimating the contribution of the BQ degradation products to the visible signal in the spectra (Fig. S9), however, at the end of 30 min under UV–vis illumination the NBB degradation was only 15%.

These results show that although both catalysts present distinct surface area, the comparable performance towards the photocatalytic degradation of NBB occurs at the expense of distinct active species, hydroxyl radical for TiO_2 and superoxide radical for BiOCl . In the case of BiOCl extra advantage was also found since its synthesis at room temperature overcomes any gain conferred by the higher surface area of TiO_2 . Also, leaving opportunity to improve the BiOCl containing sample performance by increasing its surface area through manipulation of the synthesis parameters [41,59]. On the other hand, the lower reusability found for Cot- BiOCl , may require only some improvements of the NPs attachment to the fiber surface. Nevertheless, the successful functionalization of the fibers surface by



Scheme 2. Proposed energy diagram for the charge separation process for TiO_2 and BiOCl and the degradation of NBB under UV–vis irradiation.

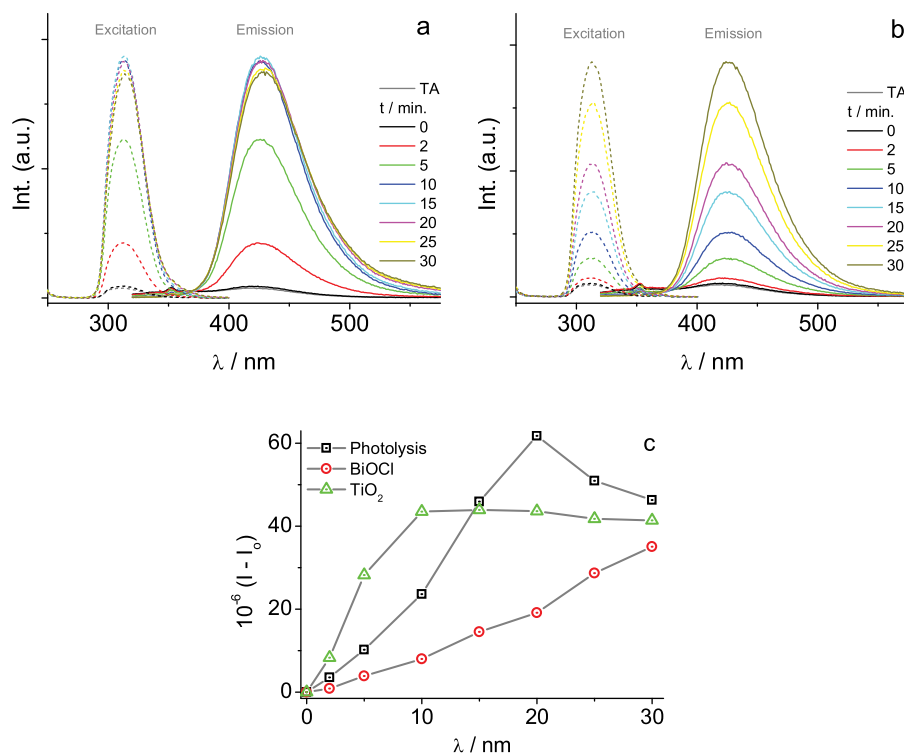


Fig. 8. Time profiles for fluorescence excitation and emission spectra for the 2-HTA production under UV-vis irradiation using (a) TiO₂ and (b) BiOCl NPs as photocatalysts, and (c) comparison with photolysis using the emission data.

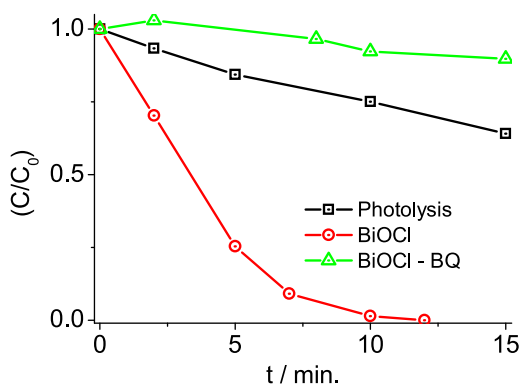


Fig. 9. Time profiles for UV-vis spectra for the photocatalytic degradation of NBB in the presence of BiOCl and 1 mM of BQ, BiOCl response without BQ and photolysis data.

immobilization of the catalyst NPs, TiO₂ and BiOCl, translates in a significant advantage; the supported catalyst is easily recovered without requiring any time-consuming centrifugation and/or another separation step.

4. Conclusions

Successful *in situ* modification of cotton fibers with semiconductor TiO₂ and BiOCl NPs was achieved. The obtained nanoparticles and modified fibers show good crystallinity and the fibers are not adversely affected by the NPs synthesis conditions, namely the high temperature used for TiO₂ synthesis and acidic medium for BiCl₃ impregnation. Uniform and continuous coating of the cotton fibers was attained with TiO₂ whereas BiOCl particles were dispersed on the surface. A small increase of the fiber surface area was observed in both cases due to the smooth layer of NPs on the

surface although TiO₂ NPs have a 10 times higher surface area than BiOCl (89.7 vs 8.8 m² g⁻¹). The effective functionalization of the fibers upon coating with NPs is corroborated by the optical response of the material with light absorption in the UV range. The photocatalytic activity of the Cot-NPs samples, evaluated by means of NBB degradation, shows high performance for the NPs coated cotton, indicating that these can be used as supported catalysts for the degradation of pollutants. It is noteworthy that in the presence of TiO₂, the main active species involved in the photodegradation process is the hydroxyl radical whereas for BiOCl it is the superoxide radical. The modified fibers are reliable for six reutilizations however mainly for BiOCl some catalyst loss may occur after the fourth cycle. The spontaneous changes of BiOCl under irradiation with a consequent activity extended to the visible range of the electromagnetic spectrum in BiOCl_{UV}, along with the simple synthesis method, performed at room temperature without need for precursors, confer to this material extra advantage as compared with TiO₂. TiO₂ displays comparable photocatalytic activity to that of BiOCl, at the expenses of high synthesis temperature and time consumption (160 °C/24 h) and not significant advantage of high surface area. Therefore, it can be concluded that BiOCl supported on cotton fibers is a promising material for photocatalysis applications.

Acknowledgement

The authors gratefully acknowledge the financial support from Fundação para a Ciência e a Tecnologia (SFRH/BPD/77404/2011, PEst-OE/QUI/UI0612/2013 and UID/MULTI/00612/2013).

Appendix A. Supplementary data

Supplementary data associated with this article can be found, in the online version, at <https://doi.org/10.1016/j.jphotochem.2018.02.032>.

References

- [1] F.M. AL-Oqla, S.M. Sapuan, Natural fiber reinforced polymer composites in industrial applications: feasibility of date palm fibers for sustainable automotive industry, *J. Clean. Prod.* 66 (2014) 347–354.
- [2] W.C. Smith (Ed.), *Smart Textile Coatings and Laminates*, Woodhead Publishing Limited and CRC Press LLC, 2010.
- [3] M. Chan, D. Estève, J.-Y. Fourniels, C. Escriba, E. Campo, Smart wearable systems: current status and future challenges, *Artif. Intell. Med.* 56 (2012) 137–156.
- [4] M. Stoppa, A. Chiolerio, Wearable electronics and smart textiles a critical review, *Sensors* 14 (2014) 11957–11992.
- [5] L. Hu, M. Pasta, F. La Mantia, L.F. Cui, S. Jeong, H.D. Deshazer, J.W. Choi, S.M. Han, Y. Cui, Stretchable, porous, and conductive energy textiles, *Nano Lett.* 10 (2010) 708–714.
- [6] S.V. Joshi, L.T. Drzal, A.K. Mohanty, S. Arora, Are natural fiber composites environmentally superior to glass fiber reinforced composites? *Composites A* 35 (2004) 371–376.
- [7] E.S. Ates, H.E. Unalan, Zinc oxide nanowire enhanced multifunctional coatings for cotton fabrics, *Thin Solid Films* 520 (2012) 4658–4661.
- [8] K. Qi, W.A. Daoud, J.H. Xin, C.L. Mak, W. Tang, W.P. Cheung, Self-cleaning cotton, *J. Mater. Chem.* 16 (2006) 4567–4574.
- [9] G. Gonçalves, P.A.A.P. Marques, R.J.B. Pinto, T. Trindade, C.P. Neto, Surface modification of cellulosic fibers for multi-purpose TiO₂ based nanocomposites, *Comp. Sci. Technol.* 69 (2009) 1051–1056.
- [10] R.M. Abdelhameed, H. Abdel-Gawad, M. Elshahat, H.E. Emam, Cu–BTC/cotton composite: design and removal of ethion insecticide from water, *RSC Adv.* 6 (2016) 42324–42333.
- [11] S. Afzal, W.A. Daoud, S.J. Langford, Superhydrophobic and photocatalytic selfcleaning cotton, *J. Mater. Chem. A* 2 (2014) 18005–18011.
- [12] Y. Yang, C. Flatebo, J. Liang, P. Dong, J. Yuan, T. Wang, J. Zhang, W. Chen, J. Wu, P. M. Ajayan, L. Ci, Q. Li, J. Lou, Towards methyl orange degradation by direct sunlight using coupled TiO₂ nanoparticles and carbonized cotton T-shirt, *Appl. Mater. Today* 3 (2016) 57–62.
- [13] M. Abid, S. Bouattour, D.S. Conceição, A.M. Ferrara, L.F.V. Ferreira, A.M. Botelho do Rego, M.R. Vilar, S. Boufi, Hybrid cotton–anatase prepared under mild conditions with high photocatalytic activity under sunlight, *RSC Adv.* 6 (2016) 58957–58969.
- [14] S. Mowafi, M. Rehan, H.M. Mashaly, A.A. El-Kheir, H.E. Emam, Influence of silver nanoparticles on the fabrics functions prepared by in-situ technique, *J. Tex. Inst.* 108 (2017) 1828–1839.
- [15] A.A. El-Sayed, M. Salama, M.H. El-Rafie, H.E. Emam, Modified rice straw as a template in syntheses of nano TiO₂ loaded on wool fibers for wastewater treatment, *J. Nat. Fib.* 14 (2017) 297–309.
- [16] H.E. Emam, N.H. Saleh, K.S. Nagy, M.K. Zahran, Instantly AgNPs deposition through facile solventless technique for poly-functional cotton fabrics, *Int. J. Biol. Macromol.* 84 (2016) 308–318.
- [17] M.I. Mejía, J.M. Marín, G. Restrepo, C. Pulgarín, E. Mielczarski, J. Mielczarski, I. Stolitchnov, J. Kiwi, Innovative UVC light (185 nm) and radio-frequency-plasma pretreatment of nylon fabrics at atmospheric pressure and their implications in photocatalytic processes, *ACS Appl. Mater. Interface* 1 (2009) 2190–2198.
- [18] M.M. Kabir, H. Wang, K.T. Lau, F. Cardona, Chemical treatments on plant-based natural fibre reinforced polymer composites: an overview, *Composites B* 43 (2012) 2883–2892.
- [19] Y.L. Lam, C.W. Kan, C.W. Yuen, C.H. Au, Low stress mechanical properties of plasma-treated cotton fabric subjected to titanium dioxide coating, *Text. Res. J.* 81 (2011) 1008–1013.
- [20] A. Yadav, V. Prasad, A.A. Kathie, S. Raj, D. Yadav, C. Sundaramoorthy, N. Vigneshwarab, Functional finishing in cotton fabrics using zinc oxide nanoparticles, *Bull. Mater. Sci.* 29 (2006) 641–645.
- [21] I. Perelshtein, G. Applert, N. Perkas, G. Guibert, S. Mikhailov, A. Gedanken, Sonochemical coating of silver nanoparticles on textile fabrics (nylon, polyester and cotton) and their antibacterial activity, *Nanotechnology* 19 (2008) 245705–245710.
- [22] V.H.T. Thi, B.-K. Lee, Development of multifunctional self-cleaning and UV blocking cotton fabric with modification of photoactive ZnO coating via microwave method, *J. Photochem. Photobiol. A* 338 (2017) 13–22.
- [23] A.L. Linsebigler, G. Lu, J.T. Yates Jr., Photocatalysis on TiO₂ surfaces: principles, mechanisms, and selected results, *Chem. Rev.* 95 (1995) 735–758.
- [24] V. Prasada, A. Arputharaja, A.K. Bharimallab, P.G. Patilb, N. Vigneshwaran, Durable multifunctional finishing of cotton fabrics by in situ synthesis of nano-ZnO, *Appl. Surf. Sci.* 390 (2016) 936–940.
- [25] M. Rastgo, M. Montazer, R.M.A. Malek, T. Harifi, M.M. Rad, Ultrasound mediation for one-pot sonosynthesis and deposition of magnetite nanoparticles on cotton/polyester fabric as a novel magnetic photocatalytic, sonocatalytic, antibacterial and antifungal textile, *Ultrasonics Sonochem.* 31 (2016) 257–266.
- [26] M. Montazer, M. Dastjerdi, M. Azdaloo, M.M. Rad, Simultaneous synthesis and fabrication of nano Cu₂O on cellulosic fabric using copper sulfate and glucose in alkali media producing safe bio- and photoactive textiles without color change, *Cellulose* 22 (2015) 4049–4064.
- [27] Z. Du, R. Guo, J. Lan, S. Jiang, S. Lin, C. Cheng, L. Zhao, Bismuth tungstate coating on polyester fabric modified with dopamine for photocatalytic property under visible light irradiation, *Surf. Coat. Technol.* 319 (2017) 219–229.
- [28] M. Koelsch, S. Cassaignon, C.T.T. Minh, J.-F. Guillemales, J.-P. Jolivet, Electrochemical comparative study of titania (anatase brookite and rutile) nanoparticles synthesized in aqueous medium, *Thin Solid Films* 451–452 (2004) 86–92.
- [29] A. Petica, C. Gaidau, M. Ignat, C. Sendrea, L. Anicai, Doped TiO₂ nanophotocatalysts for leather surface finishing with self-cleaning properties, *J. Coat. Technol. Res.* 12 (2015) 1153–1163.
- [30] A.M. Luisa, M.C. Neves, M.H. Mendonça, O.C. Monteiro, Influence of calcination parameters on the TiO₂ photocatalytic properties, *Mater. Chem. Phys.* 125 (2011) 20–25.
- [31] A. Di Paola, G. Cufalo, M. Addamo, M. Bellardita, R. Camprotrini, M. Ischia, R. Ceccato, L. Palmisano, Photocatalytic activity of nanocrystalline TiO₂ (brookite, rutile and brookite-based) powders prepared by thermohydrolysis of TiCl₄ in aqueous chloride solutions, *Colloid Surf. A* 317 (2008) 366–376.
- [32] S. Cassaignon, M. Koelsch, J.-P. Jolivet, From TiCl₃ to TiO₂ nanoparticles (anatase, brookite and rutile): thermohydrolysis and oxidation in aqueous medium, *J. Phys. Chem. Solids* 68 (2007) 695–700.
- [33] U.G. Akpan, B.H. Hameed, Parameters affecting the photocatalytic degradation of dyes using TiO₂-based photocatalysts: a review, *J. Hazard. Mater.* 170 (2009) 520–529.
- [34] O. Ola, M.M. Maroto-Valer, Review of material design and reactor engineering on TiO₂ photocatalysis for CO₂ reduction, *J. Photochem. Photobiol. C* 24 (2015) 16–42.
- [35] S. Das, R. Zazpe, J. Prikryl, P. Knotek, M. Krbal, H. Sopha, V. Podzemna, J.M. Macak, Influence of annealing temperatures on the properties of low aspect-ratio TiO₂ nanotube layers, *Electrochim. Acta* 213 (2016) 452–459.
- [36] L. Sun, Y. Qin, Q. Cao, B. Hu, Z. Huang, L. Ye, X. Tang, Novel photocatalytic antibacterial activity of TiO₂ microspheres exposing 100% reactive {111} facets, *Chem. Commun.* 47 (2011) 12628–12630.
- [37] K. Zhou, Y. Zhu, X. Yang, X. Jiang, C. Li, Preparation of graphene-TiO₂ composites with enhanced photocatalytic activity, *New J. Chem.* 35 (2011) 353–359.
- [38] J. Schneider, M. Matsuoka, M. Takeuchi, J. Zhang, Y. Horiuchi, M. Anpo, D.W. Bahnemann, Understanding TiO₂ photocatalysis: mechanisms and materials, *Chem. Rev.* 114 (2014) 9919–9986.
- [39] S. Buddee, S. Wongnawa, P. Sriprang, C. Sriwong, Curcumin-sensitized TiO₂ for enhanced photodegradation of dyes under visible light, *J. Nanopart. Res.* 16 (2014) 2336–2346.
- [40] H. Zhao, Y. Zhang, G. Li, F. Tian, H. Tang, R. Chen, Rhodamine B-sensitized BiOCl hierarchical nanostructure for methyl orange photodegradation, *RSC Adv.* 6 (2016) 7772–7779.
- [41] L. Ye, L. Zan, L. Tian, T. Peng, J. Zhang, The {001} facets-dependent high photoactivity of BiOCl nanosheets, *Chem. Commun.* 47 (2011) 6951–6953.
- [42] C. Tan, G. Zhu, M. Hojamberdiev, K. Okada, J. Liang, Co₃O₄ nanoparticles-loaded BiOCl nanoplates with the dominant {001} facets: efficient photodegradation of organic dyes under visible light, *Appl. Catal. B* 152–153 (2014) 425–436.
- [43] R. Tanwar, S. Kumar, U.K. Mandal, Photocatalytic activity of PAni/Fe⁰ doped BiOCl under visible light-degradation of Congo red dye, *J. Photochem. Photobiol. A* 333 (2017) 105–116.
- [44] Z. Jiang, Y. Liu, T. Jing, B. Huang, Z. Wang, X. Zhang, X. Qin, Y. Dai, One-pot solvothermal synthesis of S doped BiOCl for solar water oxidation, *RSC Adv.* 5 (2015) 47261–47264.
- [45] Y. Li, Y. Tiang, R. Zhang, L. Ma, C. Zhou, X. Tian, Hierarchical BiOCl microspheres with narrow band gap as visible light active photocatalysts, *Inorg. Chim. Acta* 439 (2016) 123–129.
- [46] G. Li, B. Jiang, S. Xiao, Z. Lian, D. Zhang, J.C. Yu, H. Li, An efficient dye-sensitized BiOCl photocatalyst for air and water purification under visible light irradiation, *Environ. Sci. Process. Impacts* 16 (2014) 1975–1980.
- [47] M. Sun, Q. Zhao, C. Du, Z. Liu, Enhanced visible light photocatalytic activity in BiOCl/SnO₂: heterojunction of two wide band-gap semiconductors, *RSC Adv.* 5 (2015) 22740–22752.
- [48] V.C. Ferreira, M.C. Neves, A.R. Hillman, O.C. Monteiro, Novel one-pot synthesis and sensitisation of new BiOCl–Bi₂S₃ nanostructures from DES medium displaying high photocatalytic activity, *RSC Adv.* 6 (2016) 77329–77339.
- [49] T.-W. Tzeng, S.-L. Wang, C.-C. Chen, C.-C. Tan, Y.-T. Liu, T.-Y. Chen, Y.-M. Tzou, C. C. Chene, J.T. Hung, Photolysis and photocatalytic decomposition of sulfamethazine antibiotics in an aqueous solution with TiO₂, *RSC Adv.* 6 (2016) 69301–69310.
- [50] C.P. Sajan, S. Wageh, A.A. Al-Ghamdi, J. Yu, S. Cao, TiO₂ nanosheets with exposed {001} facets for photocatalytic applications, *Nano Res.* 9 (2016) 3–27.
- [51] N. Koutahzadeh, M.R. Esfahania, P.E. Arce, Removal of Acid Black 1 from water by the pulsed corona discharge advanced oxidation method, *J. Water Proc. Eng.* 10 (2016) 1–8.
- [52] G. Mamba, X.Y. Mbianda, A.K. Mishra, Photocatalytic degradation of the diazo dye naphthol blue black in water using MWCNT/Gd,N,S-TiO₂ nanocomposites under simulated solar light, *J. Environ. Sci.* 33 (2015) 219–228.
- [53] Y. Zhai, S. Zhang, H. Pang, Preparation, characterization and photocatalytic activity of CeO₂ nanocrystalline using ammonium bicarbonate as precipitant, *Mater. Lett.* 61 (2007) 1863–1866.
- [54] P. Borker, A.V. Salker, Solar assisted photocatalytic degradation of Naphthol Blue Black dye using Ce_{1-x}Mn_xO₂, *Mater. Chem. Phys.* 103 (2007) 366–370.
- [55] M.K. Yakubu, S.M. Gumel, L.O. Ogbore, A.T. Adekunle, Pretreatment of cotton fibres with alcohols to optimize dye uptake, *Casp. J. Env. Sci.* 4 (2006) 39–44.
- [56] M.R. Nunes, O.C. Monteiro, A.L. Castro, D.A. Vasconcelos, A.J. Silvestre, A new chemical route to synthesise TM-doped (TM = Co, Fe) TiO₂ nanoparticles, *Eur. J. Inorg. Chem.* (2008) 961–965.

- [57] E.K. Ylhainen, M.R. Nunes, A.J. Silvestre, O.C. Monteiro, Synthesis of titanate nanostructures using amorphous precursor material and their adsorption/photocatalytic properties, *J. Mater. Sci.* 47 (2012) 4305–4312.
- [58] T.J. Entradas, J.F. Cabrita, B. Barrocas, M.R. Nunes, A.J. Silvestre, O.C. Monteiro, Synthesis of titanate nanofibers co-sensitized with ZnS and Bi₂S₃ nanocrystallites and their application on pollutants removal, *Mater. Res. Bull.* 72 (2015) 20–28.
- [59] K. Zhang, J. Liang, S. Wang, J. Liu, K. Ren, X. Zheng, H. Luo, Y. Peng, X. Zuo, X. Bo, J. Li, X. Yu, BiOCl sub-microcrystals induced by citric acid and their high photocatalytic activities, *Cryst. Growth Des.* 12 (2012) 793–803.
- [60] O.C. Monteiro, M.C. Neves, T. Trindade, Zinc sulfide nanocoating of silica submicron spheres using a single-source method, *J. Nanosci. Nanotechnol.* 4 (2004) 146–150.
- [61] V.C. Ferreira, M.R. Nunes, A.J. Silvestre, O.C. Monteiro, Synthesis and properties of Co-doped titanate nanotubes and their optical sensitization with methylene blue, *Mater. Chem. Phys.* 142 (2013) 355–362.
- [62] N. Barbero, D. Vione, Why dyes should not be used to test the photocatalytic activity of semiconductor oxides, *Environ. Sci. Technol.* 50 (2016) 2130–2131.
- [63] E. Kordouli, K. Bourikas, A. Lycourghiotis, C. Kordulisa, The mechanism of azo-dyes adsorption on the titanium dioxide surface and their photocatalytic degradation over samples with various anatase/rutile ratios, *Catal. Today* 252 (2015) 128–135.
- [64] J. Miao, H.-B. Lu, D. Habibi, M.H. Khiadani, L.-C. Zhang, Photocatalytic degradation of the azo dye acid red 14 in nanosized TiO₂ suspension under simulated solar light, *Clean – Soil Air Water* 43 (2015) 1037–1043.
- [65] K. Stana-Kleinschek, V. Ribitsch, Electrokinetic properties of processed cellulose fibers, *Coll. Surf. A* 140 (1998) 127–138.
- [66] I. Bickley, T. Gonzalez-Carreno, J.S. Lees, L. Palmisano, R.J.D. Tilley, A structural investigation of titanium dioxide photocatalysts, *J. Solid State Chem.* 92 (1991) 178–190.
- [67] L. Ye, K. Deng, F. Xu, L. Tian, T. Peng, L. Zan, Increasing visible-light absorption for photocatalysis with black BiOCl, *Phys. Chem. Chem. Phys.* 14 (2012) 82–85.
- [68] Y. Liu, G. Ji, M.A. Dastageer, L. Zhu, J. Wang, B. Zhang, X. Chang, M.A. Gondal, Highly-active direct Z-scheme Si/TiO₂ photocatalyst for boosted CO₂ reduction into value-added methanol, *RSC Adv.* 4 (2014) 56961–56969.
- [69] H. Cheng, B. Huang, X. Qin, X. Zhang, Y. Dai, A controlled anion exchange strategy to synthesize Bi₂S₃ nanocrystals/BiOCl hybrid architectures with efficient visible light photoactivity, *Chem. Commun.* 48 (2012) 97–99.
- [70] R.G. Pearson, Absolute electronegativity and hardness: application to inorganic chemistry, *Inorg. Chem.* 27 (1988) 734–740.
- [71] L. Leonal, G. Sbarcea, I.V. Branzoi, Cyclic voltammetry for energy levels estimation of organic materials, *U.P.B. Sci. Bull. Ser. B* 75 (2013) 111–118.
- [72] C.M. Cardona, W. Li, A.E. Kaifer, D. Stockdale, G.C. Bazan, Electrochemical considerations for determining absolute frontier orbital energy levels of conjugated polymers for solar cell applications, *Adv. Mater.* 23 (2011) 2367–2371.
- [73] X.H. Lin, S.N. Lee, W. Zhang, S.F.Y. Li, Photocatalytic degradation of terephthalic acid on sulfated titania particles and identification of fluorescent intermediates, *J. Hazard. Mater.* 303 (2016) 64–75.
- [74] B. Chládková, E. Evgenidou, L. Kvítek, A. Panáček, R. Zboril, P. Kovár, D. Lambropoulou, Adsorption and photocatalysis of nanocrystalline TiO₂ particles for Reactive Red 195 removal: effect of humic acids, anions and scavengers, *Environ. Sci. Pollut. Res.* 22 (2015) 16514–16524.
- [75] J. Hu, W. Fan, W. Ye, C. Huang, X. Qiu, Insights into the photosensitivity activity of BiOCl under visible light irradiation, *Appl. Catal. B* 158–159 (2014) 182–189.
- [76] L. Lei, H. Jin, Q. Zhang, J. Xu, D. Gao, Z. Fu, A novel enhanced visible-light-driven photocatalyst via hybridization of nanosized BiOCl and graphitic C₃N₄, *Dalton Trans.* 44 (2015) 795–803.
- [77] Y. Mia, L. Wen, Z. Wang, D. Cao, Y. Fang, Y. Lei, Building of anti-restack 3D BiOCl hierarchy by ultrathin nanosheets towards enhanced photocatalytic activity, *Appl. Catal. B* 176–177 (2015) 331–337.
- [78] J. Song, Q. Fan, W. Zhu, R. Wang, Z. Dong, Preparation of BiOCl with high specific surface area and excellent visible light photocatalytic activity, *Mater. Lett.* 165 (2016) 14–18.
- [79] M.A. Gondala, X. Chang, M.A. Ali, Z.H. Yaman, Q. Zhou, G. Ji, Adsorption and degradation performance of Rhodamine B over BiOBr under monochromatic 532 nm pulsed laser exposure, *Appl. Catal. A* 397 (2011) 192–200.
- [80] L. Ye, J. Chen, L. Tian, J. Liu, T. Peng, K. Deng, L. Zan, BiOI thin film via chemical vapor transport: photocatalytic activity durability, selectivity and mechanism, *Appl. Catal. B* 130–131 (2013) 1–7.